



**AIAA 2002-0802**

**Broadband Noise Predictions Based  
on a New Aeroacoustic Formulation**

J. Casper and F. Farassat  
NASA Langley Research Center  
Hampton, VA

**40th Aerospace Sciences  
Meeting and Exhibit**  
January 14-17, 2002 / Reno, NV

# BROADBAND NOISE PREDICTIONS BASED ON A NEW AEROACOUSTIC FORMULATION

J. Casper\* and F. Farassat†  
NASA Langley Research Center  
Hampton, VA 23681

## Abstract

A new analytic result in acoustics called "Formulation 1B," proposed by Farassat, is used to compute the loading noise from an unsteady surface pressure distribution on a thin airfoil in the time domain. This formulation is a new solution of the Ffowcs Williams-Hawkings equation with the loading source term. The formulation contains a far-field surface integral that depends on the time derivative and the surface gradient of the pressure on the airfoil, as well as a contour integral on the boundary of the airfoil surface. As a first test case, the new formulation is used to compute the noise radiated from a flat plate, moving through a sinusoidal gust of constant frequency. The unsteady surface pressure for this test case is specified analytically from a result that is based on linear airfoil theory. This test case is used to examine the velocity scaling properties of Formulation 1B, and to demonstrate its equivalence to Formulation 1A, of Farassat. The new acoustic formulation, again with an analytic surface pressure, is then used to predict broadband noise radiated from an airfoil immersed in homogeneous turbulence. The results are compared with experimental data previously reported by Paterson and Amiet. Good agreement between predictions and measurements is obtained. The predicted results also agree very well with those of Paterson and Amiet, who used a frequency-domain approach. Finally, an alternative form of Formulation 1B is described for statistical analysis of broadband noise.

## Nomenclature

$b$	= airfoil semi-span (m)
$c_0$	= ambient sound speed (m/sec)
$f$	= frequency (Hz)
$\tilde{f}$	= geometry function for airfoil surface
$\tilde{F}$	= $\tilde{f}$ observed in retarded time (Eq. 2(b))
$E^*$	= combination of Fresnel integrals (Eq. 9(g))
$g$	= velocity-to-pressure transfer function
$k$	= $\omega/U$ , convective wave number ( $m^{-1}$ )
$\bar{k}$	= $kL_c/2$ , reduced frequency
$L_c$	= airfoil chord (m)
$\mathcal{L}_1$	= stream-wise integral length scale
$l_i$	= correlation length in the "i" direction

$\vec{M}$	= $\vec{V}/c_0$ , Mach number vector
$M_r$	= $\vec{M} \cdot \vec{r}/r$ Mach number in radiation direction
$M_\nu$	= $\vec{M} \cdot \hat{\nu}$ Mach number in direction of $\hat{\nu}$
$p$	= unsteady pressure on upper airfoil surface (Pa)
$p'$	= sound pressure radiated to observer (Pa)
$\partial p/\partial s$	= directional surface pressure gradient (Pa/m)
$\vec{r}$	= $\vec{x} - \vec{y}$ , sound radiation vector (m)
$R_{uu}$	= correlation function of $u$
$S_{uu}$	= spectral density of $u$
$t$	= observer time (sec)
$U$	= uniform free-stream speed (m/sec)
$u$	= unsteady stream-wise velocity (m/sec)
$\vec{V}$	= airfoil velocity vector (m/sec)
$V$	= local velocity vector magnitude (m/sec)
$w$	= unsteady upwash velocity (m/sec)
$\vec{x}$	= $[x_1, x_2, x_3]^T$ , observer position (Fig. 1)
$\vec{y}$	= $[y_1, y_2, 0]^T$ , surface source position (Fig. 1)
$\beta$	= $\sqrt{1 - M^2}$
$\lambda$	= $c_0/f$ , acoustic wave-length (m)
$\mu$	= $M \bar{k}/\beta^2$
$\psi$	= directivity angle (Fig. 5)
$\hat{\nu}$	= unit, inward geodesic normal (Fig. 1)
$\theta$	= radiation direction (Fig. 1)
$\rho_0$	= ambient density ( $kg/m^3$ )
$\tau$	= $t - r/c_0$ , source time (sec)
$\Phi$	= random phase variable
$\omega$	= $2\pi f$ , circular frequency (Hz)

## 1. Introduction

The development of analytical methods to predict noise radiated from an airflow over a rigid body has been a subject of extensive research within the aeroacoustic community for decades. Research in this area has, in large part, been motivated by the desire to incorporate the results of aeroacoustic analysis into an aerodynamic design methodology. The present work is similarly motivated, and the resulting formulation should lend itself well to an engineering design-tool suite.

The current work is specifically focused on the calculation of far-field noise that results from fluctuating pressure on a solid surface. The acoustic analogy<sup>1</sup> provides a framework for the development of methods to predict noise from many types of sources, including noise due to unsteady surface loading. Such noise is mathematically described by the loading source term, or "dipole term," of the Ffowcs Williams-Hawkings (FW-H) equation.<sup>2</sup> Because the noise due to an airflow over a rigid surface is often dominated by dipole radiation, the acoustic formulations of interest in this work are determined by solutions of the FW-H equation with the loading source term, *i.e.* neglecting the

Copyright © 2002 by the American Institute of Aeronautics and Astronautics, Inc. No copyright is asserted in the United States under Title 17, U.S. Code. The U.S. Government has a royalty-free license to exercise all rights under the copyright claimed herein for Governmental Purposes. All other rights are reserved by the copyright owner.

\* Research Scientist, Computational Modeling and Simulation Branch, AIAA Senior Member

† Senior Research Scientist, Aeroacoustics Branch, AIAA Assoc. Fellow

thickness and quadrupole terms.

The solution of the FW-H equation can be written in many forms. A new solution, called “Formulation 1B” is presented herein. The types of noise that can be calculated with the proposed Formulation 1B are most types of broadband noise, including noise that is dominated by an airfoil’s leading and trailing edges. Formulation 1B is the simplest loading-noise prediction formula known to date. This simplicity makes the new formulation highly suitable for statistical analysis of broadband noise for rotating surfaces.

In Section 2, Formulation 1B is derived for the specific case of a flat plate in rectilinear motion. For low Mach numbers and distant observers, the dominant term in this formulation is a far-field surface integral that depends on the time derivative and the surface gradient of the airfoil surface pressure. The formulation also contains a contour integral on the boundary of the airfoil surface that includes the leading and trailing edges. This line integral vanishes along the trailing edge if the Kutta condition is imposed.

In Section 3, Formulation 1B is used to calculate the noise radiated from a flat plate moving through a sinusoidal gust of constant frequency. The unsteady surface pressure used in this test case is an analytical result from linearized airfoil theory that is taken from the work of Amiet.<sup>3,4</sup> A mesh refinement study is performed to demonstrate the equivalence of Formulation 1B with Formulation 1A,<sup>5</sup> a previously developed acoustic formulation that is also a solution of the FW-H equation. Results from this analytical test case are also used to examine the velocity scaling properties of Formulation 1B, which are found to be consistent with the results of Curle<sup>6</sup> and Ffowcs Williams and Hall.<sup>7</sup> The directivity of the noise induced by a periodic gust is also examined.

In Section 4, the single-frequency surface pressure in Section 3 is extended by spectral representation to serve as an analytic broadband source model for incident turbulence noise. This surface pressure is used as input to Formulation 1B to predict broadband noise to the far field. The resulting calculations are compared to experimental data previously reported by Paterson and Amiet.<sup>8</sup> In Section 5, an alternative acoustic formulation is described for statistical analysis of broadband noise.

## 2. Acoustic Formulation

Consider a flat, finite surface moving in the plane  $x_3=0$  along a velocity vector  $\vec{V}$ . Let  $\tilde{f}(x_1, x_2, t)$  denote a geometric function that is so defined that  $\tilde{f} = 0$  on the surface edge, and  $\tilde{f} > 0$  on the interior of the surface. Let  $\hat{\nu} = \vec{\nabla} \tilde{f}$  denote the unit geodesic normal which lies in the plane of the surface, is normal to the edge, and is directed inward (See Fig. 1). The velocity vector  $\vec{V}$  and the plate’s geometry are related to the coordinate axes as pictured in Fig. 1. Note that  $\vec{V}$  need not be constant in space or time. The only stipulation on the velocity is that the motion of the surface is in the same plane as the surface.

Denote by  $\vec{x} = [x_1, x_2, x_3]^T$  the position of an observer, and by  $\vec{y} = [y_1, y_2, 0]^T$  the position of a source point on the plate’s surface (Fig. 1). The unsteady perturbation pressure  $p(\vec{y}, t)$  on the surface gives rise to sound that radiates along  $\vec{r} = \vec{x} - \vec{y}$  to the observer. This sound is described by

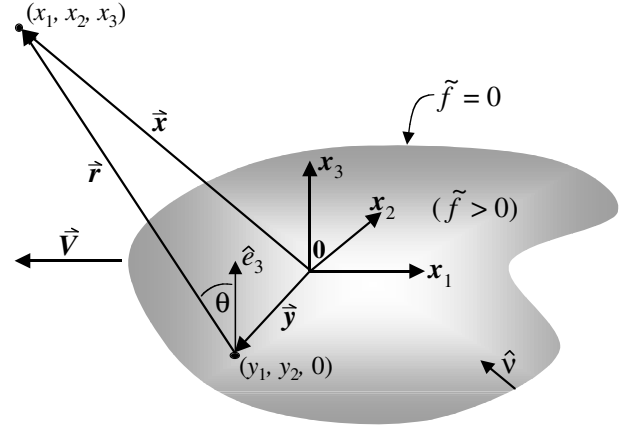


Fig. 1 Schematic for the derivation of Formulation 1B.

$p'(\vec{x}, t)$ , the perturbation pressure that arrives at the point  $(x_1, x_2, x_3)$  at time  $t$ . Both  $\vec{x}$  and  $\vec{y}$  frames of reference are considered fixed relative to the undisturbed medium. For some of the subtle mathematical details in the following derivation, see Ref. 9.

From the FW-H equation, the loading noise is given by a solution of

$$\frac{1}{c_0^2} \frac{\partial^2 p'}{\partial t^2} - \nabla^2 p' = -\vec{\nabla} \cdot [p \hat{n} H(\tilde{f}) \delta(x_3)] \quad (1a)$$

where  $c_0$  is the ambient sound speed and  $\hat{n}$  is the unit surface normal which, for the present case, is equivalent to  $\hat{e}_3$ , the unit vector in the direction of the  $x_3$ -axis.  $H$  is the Heaviside step function and  $\delta$  the Dirac delta function. Evaluating the divergence in Eq. 1(a) yields

$$\frac{1}{c_0^2} \frac{\partial^2 p'}{\partial t^2} - \nabla^2 p' = -p(x_1, x_2, t) H(\tilde{f}) \delta'(x_3) \quad (1b)$$

where  $\delta'(x_3)$  denotes differentiation with respect to  $x_3$ .

Eq. 1(b) is the wave equation with a source term, and its formal solution in an unbounded domain requires the Green’s function  $\delta(g)/4\pi r$ , where  $g = \tau - t + r/c_0$ , and  $t$  and  $\tau$  are the observer and source times, respectively. The solution of Eq. 1(b) can then be written in the form

$$4\pi p'(\vec{x}, t) = - \int_{-\infty}^t \int_{\mathbb{R}^3} \frac{\delta(g)}{r} p(y_1, y_2, \tau) H(\tilde{f}) \delta'(y_3) d\vec{y} d\tau$$

Now, let  $\tau \rightarrow g$  and integrate with respect to  $g$ . The result can be written

$$4\pi p'(\vec{x}, t) = - \int_{\mathbb{R}^3} \frac{1}{r} [p]_{\text{ret}} H(\tilde{F}) \delta'(y_3) d\vec{y} \quad (2a)$$

where the subscript “ret” denotes evaluation at retarded time  $\tau = t - r/c_0$ , and  $\tilde{F}$  is

$$\tilde{F}(y_1, y_2; \vec{x}, t) = \tilde{f}(y_1, y_2, t - r/c_0) = [\tilde{f}]_{\text{ret}} \quad (2b)$$

Integration with respect to  $y_3$  on the right-hand side of Eq. 2(a) yields

$$4\pi p'(\vec{x}, t) = - \int_{\mathbb{R}^2} \frac{\partial}{\partial y_3} \left\{ \frac{[p]_{\text{ret}}}{r} H(\tilde{F}) \right\}_{y_3=0} dy_1 dy_2 \quad (3a)$$

Performing the differentiation in the integrand of Eq. 3(a) yields

$$\begin{aligned} \frac{\partial}{\partial y_3} \left\{ \frac{[p]_{\text{ret}}}{r} H(\tilde{F}) \right\} &= \frac{1}{c_0 r} [\hat{r}_3 \dot{p}]_{\text{ret}} H(\tilde{F}) \\ &+ \frac{1}{r^2} [\hat{r}_3 p]_{\text{ret}} H(\tilde{F}) \\ &+ \frac{1}{c_0 r} \left[ \frac{\partial \tilde{f}}{\partial \tau} \hat{r}_3 p \right]_{\text{ret}} \delta(\tilde{F}) \end{aligned} \quad (3b)$$

where  $\dot{p}$  is the time derivative of pressure evaluated relative to an observer that is fixed with respect to the medium at rest, and  $\hat{r}_3$  is the third component of the unit radiation vector  $\hat{\mathbf{r}} = \vec{r}/r$ . Clearly, then,  $\hat{r}_3 = \hat{\mathbf{e}}_3 \cdot \hat{\mathbf{r}} = \cos \theta$ , where  $\theta$  is as shown in Fig. 1. The first and second terms on the right-hand side of Eq. 3(b) are of the similar form  $Q H(\tilde{F})$ . In Ref. 10, it is shown that the integration of these two terms in Eq. 3(a) can be written

$$\int_{\mathbb{R}^2} Q H(\tilde{F}) dy_1 dy_2 = \int_{\tilde{F} > 0} Q d\Sigma = \int_{\tilde{f} > 0} \frac{Q}{[1 - M_r]_{\text{ret}}} dS \quad (4a)$$

where  $d\Sigma$  is the element of the surface area of the acoustic planform of  $\tilde{f} > 0$ . Also,  $M_r = \vec{M} \cdot \hat{\mathbf{r}}$  is the Mach number in the radiation direction, where  $\vec{M} = \vec{V}/c_0$  is the local Mach number vector of the surface.

The integrated value of the third term on the right-hand side of Eq. 3(b) is determined as follows. This integral is of the form

$$\mathcal{I} = \int_{\mathbb{R}^2} q(y_1, y_2) \delta(\tilde{F}) dy_1 dy_2 \quad (4b)$$

The differential surface element  $dy_1 dy_2$  can be written<sup>10</sup>

$$dy_1 dy_2 = d\mathcal{L} d\mathcal{N} = \frac{d\mathcal{L} d\tilde{F}}{|\nabla_2 \tilde{F}|} \quad (4c)$$

where  $d\mathcal{L}$  and  $d\mathcal{N}$  are differential elements of arclength that are, respectively, parallel and normal to the the surface edge defined by  $\tilde{F} = 0$ , as shown in Fig. 2. The notation  $\nabla_2$  denotes the surface gradient in the  $y_1 y_2$ -plane. Moreover, it can be shown<sup>10</sup> that

$$\frac{d\mathcal{L}}{|\nabla_2 \tilde{F}|} = \frac{d\ell}{[1 - M_r]_{\text{ret}}} \quad (4d)$$

where  $d\ell$  is an element of arclength along the surface edge defined by  $\tilde{f} = 0$ . Eq. 4(b) can now be written

$$\begin{aligned} \mathcal{I} &= \int_{\mathbb{R}^2} q(y_1, y_2) \delta(\tilde{F}) \frac{d\mathcal{L} d\tilde{F}}{|\nabla_2 \tilde{F}|} \\ &= \int_{\tilde{F}=0} \frac{q(y_1, y_2)}{|\nabla_2 \tilde{F}|} d\mathcal{L} \\ &= \int_{\tilde{f}=0} \frac{q(y_1, y_2)}{[1 - M_r]_{\text{ret}}} d\ell \end{aligned} \quad (4e)$$

Note that the surface time derivative  $\partial \tilde{f} / \partial \tau$  in Eq. 3(b), and contained in  $q(y_1, y_2)$  in Eq. 4(e), is referenced to the undisturbed medium. However,  $\partial \tilde{f} / \partial \tau$  can be related to the material derivative  $D\tilde{f} / D\tau$  in the reference frame of the moving surface, by

$$\left. \frac{D\tilde{f}}{D\tau} \right|_{\tilde{f}=0} = \frac{\partial \tilde{f}}{\partial \tau} + \vec{V} \cdot \vec{\nabla} \tilde{f} = \frac{\partial \tilde{f}}{\partial \tau} + \vec{V} \cdot \hat{\nu} \quad (5a)$$

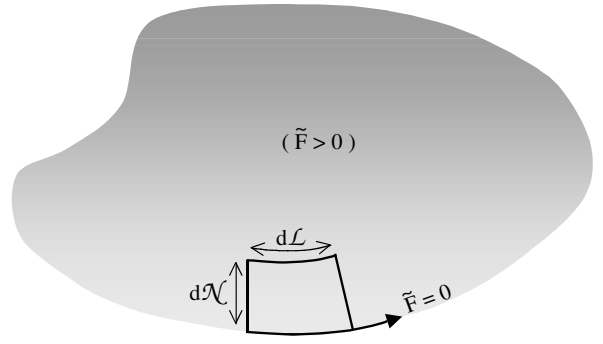


Fig. 2 Differential surface element in Eq. 4(c).

where the subscript “ $\tilde{f} = 0$ ” denotes the reference frame of the moving surface. Furthermore, when referenced to the moving surface,  $D\tilde{f} / D\tau$  must be zero, and it follows from Eq. 5(a) that  $\partial \tilde{f} / \partial \tau = -\vec{V} \cdot \hat{\nu}$ .

All three terms on the right-hand side of Eq. 3(b) are now integrated in Eq. 3(a) over the physical surface  $\tilde{f}(x_1, x_2, t) \geq 0$ , using 4(a) and 4(e). Before writing the final solution to Eq. 1(a), note that  $\dot{p}$  is referenced to the medium at rest, *e.g.* as measured by a transducer that remains stationary as the surface passes by it. The quantity  $\dot{p}$  can be related to  $\partial p / \partial \tau$ , the time derivative of pressure in the reference frame of the moving surface, *e.g.* as measured by a transducer attached to the surface. This relation is

$$\dot{p} = \frac{\partial p}{\partial \tau} + \vec{V} \cdot \vec{\nabla} p = \frac{\partial p}{\partial \tau} - V \frac{\partial p}{\partial s} \quad (5b)$$

where  $\partial p / \partial s$  is the gradient of  $p$  in the direction of  $\vec{V}$ , and  $V$  is the local magnitude of  $\vec{V}$ . The minus sign in Eq. 5(b) results from the fact that the surface gradient and velocity are measured from opposite directions (Fig. 1).

Incorporating all of the above results into Eqs. 3(a,b), the solution of Eq. 1(a) can now be written. The result is Formulation 1B,

$$\begin{aligned} 4\pi p'(\vec{x}, t) &= \int_{\tilde{f} > 0} \left[ \frac{(\partial p / \partial \tau - V \partial p / \partial s) \cos \theta}{c_0 r (1 - M_r)} \right]_{\text{ret}} dS \\ &+ \int_{\tilde{f} > 0} \left[ \frac{p \cos \theta}{r^2 (1 - M_r)} \right]_{\text{ret}} dS \\ &- \int_{\tilde{f} = 0} \left[ \frac{M_\nu p \cos \theta}{r (1 - M_r)} \right]_{\text{ret}} d\ell, \end{aligned} \quad (6)$$

where  $M_\nu = \vec{M} \cdot \hat{\nu}$ , the Mach number in the direction of  $\hat{\nu}$ .

The first and third integrals in Eq. 6 represent the sound radiated to the far field, whereas the second integral represents radiation to the near field. It is noteworthy to consider the relative contributions of the terms in Eq. 6, under the conditions of low Mach number and an observer in the acoustic far-field, *i.e.*

$$M \ll 1, \quad r \gg \lambda \quad (7)$$

where  $\lambda$  is a typical acoustic wavelength of interest. With respect to  $M$  and  $r$ , the surface far-field integral, *i.e.* the first integral in Eq. 6, is proportional to  $1/r$ , whereas the second and third integrals are proportional to  $1/r^2$  and  $M/r$ , respectively. Therefore, the far-field surface integral dominates the signal under the conditions in Eq. 7.

Note, again, that Eq. 6 is valid for the case of non-uniform flow. Therefore, Eq. 6 can be used, as is, to predict loading noise from rotating surfaces. Its predecessor, Formulation 1A,<sup>5</sup> is significantly more complicated in its rotational form, and cannot be approximated by only one surface integral in the far field. Such a significant simplification for far-field calculations makes Formulation 1B more suitable for statistical analysis of broadband sources for rotating surfaces. A statistical formulation based on Eq. 6 will be addressed in Section 5. However, the focus of the current work is the time-domain application of Formulation 1B, as will be demonstrated in the following two sections.

### 3. Sinusoidal Gust of Constant Frequency

Any noise prediction made with Eq. 6 will be only as good as the input surface pressure  $p(\vec{y}, t)$ . The current thinking is that such time-dependent pressure data would result from experimental measurement or a computational fluid dynamics (CFD) calculation. However, in this initial work, an analytic expression is used for  $p(\vec{y}, t)$  to serve as input data for the new acoustic formulation. To this end, an analytic formulation from thin-airfoil theory will be used to describe the unsteady surface pressure that results from a sinusoidal gust of constant frequency. This particular surface pressure formulation is chosen as an example that will be used in this section to establish the equivalence of Formulation 1B and Formulation 1A<sup>5</sup> and to examine the velocity scaling properties of Formulation 1B. In addition, the frequency-dependent directivity of the far-field sound produced by this sinusoidal gust is discussed.

#### 3.1 Surface Pressure from Thin Airfoil Theory

Consider a rectangular flat plate, in rectilinear motion, as in Fig. 3. The velocity vector  $\vec{V} = [-U, 0, 0]^T$ , where  $U$  is a constant subsonic speed. For the following examples, the plate's surface and its boundary,  $\vec{f} \geq 0$ , are defined by  $\{0 \leq x_1 \leq L_c\} \times \{-b \leq x_2 \leq b\}$ . This surface will be presumed to have an unsteady pressure distribution that is analytically prescribed from linearized airfoil theory, as discussed below.

In Refs. 3 and 4, Amiet presents closed-form expressions for the unsteady pressure on the surface of an infinite-span, thin airfoil. The airfoil is presumed to move rectilinearly

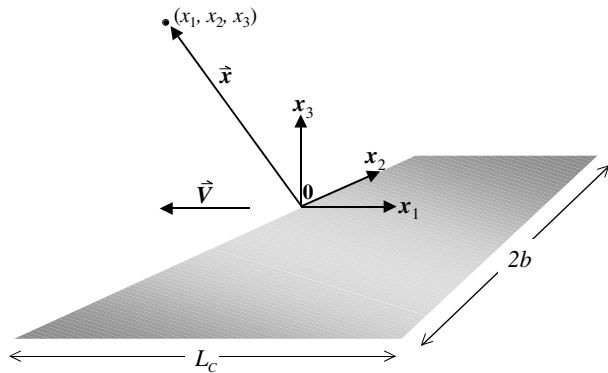


**Fig. 3** Schematic for the constant-frequency loading noise problem in Section 3.

through a sinusoidal gust. Analytical methods are used to solve the two-dimensional, time-dependent linear potential equation by representing the solution as a product of spatial and temporal solutions. The solution is represented as a truncated series in which higher-order terms are neglected (See Refs. 3 and 4 for details.).

A complex-valued representation for the airfoil surface pressure is assumed to arise from a stationary gust in one spatial dimension. This gust can be written in the “stationary” variable  $x_1 - Ut$  as

$$w(x_1 - Ut) = w_0 e^{-ik(x_1 - Ut)} \quad (8)$$

where  $k = \omega/U$  is the stream-wise convective wave number, and  $w_0$  is the gust amplitude. This gust and the airfoil surface pressure that it generates are, for now, considered as functions of a single amplitude and frequency.

The unsteady surface pressure that arises due to the incidence of a gust of the form in Eq. 8 can be written

$$\Delta P(x_1, t) = \rho_0 U w_0 g(x_1, \bar{k}) e^{ikUt} \quad (9a)$$

where  $\rho_0$  is the ambient density,  $\bar{k} = kL_c/2$  is the reduced frequency (based on the semi-chord), and  $g(x_1, \bar{k})$  is a transfer function whose form is dependent on the frequency of interest. In Ref. 8, the suggested parameter to delineate between the low and high frequency regimes is  $\mu = M\bar{k}/\beta^2$ , where  $\beta = \sqrt{1 - M^2}$ .

For low frequencies,  $\mu < 0.4$ , the transfer function is

$$g(x_1, \bar{k}) = \frac{1}{\beta} \left( \frac{L_c}{x_1} - 1 \right)^{\frac{1}{2}} G_S(\bar{k}^*) e^{i\bar{k}^* q(x_1, M)}, \quad \mu < 0.4, \quad (9b)$$

where  $\bar{k}^* = \bar{k}/\beta^2$ ,  $G_S$  is the classical Sears function,<sup>11</sup> which, for the present work, is approximated by

$$G_S(\bar{k}^*) \approx \left[ \frac{1}{1 + 2.4\bar{k}^*} + 2\pi\bar{k}^* \right]^{-\frac{1}{2}}, \quad (9c)$$

as suggested in Ref. 8, and

$$q(x_1, M) = M^2(2x_1/L_c - 1) + (1 - \beta) \ln M + \beta \ln(1 + \beta) - \ln 2 \quad (9d)$$

For high frequencies,  $\mu \geq 0.4$ , the transfer function is the sum of a leading-edge solution and a trailing-edge correction,<sup>4</sup> i.e.

$$g(x_1, \bar{k}) = (g_1 + g_2) e^{-i[2\mu(1-M)x_1/L_c + \pi/4]}, \quad \mu \geq 0.4 \quad (9e)$$

where

$$g_1(x_1, \bar{k}) = \frac{1}{[2\pi\bar{k}x_1(1+M)/L_c]^{\frac{1}{2}}} \quad (9f)$$

$$g_2(x_1, \bar{k}) = \frac{-1 + (1+i)E^*[4\mu(1-x_1/L_c)]}{[2\pi\bar{k}(1+M)]^{\frac{1}{2}}}$$

and

$$E^*(\xi) = \int_0^\xi \frac{e^{-iu}}{(2\pi u)^{\frac{1}{2}}} du \equiv \mathcal{C}(\xi) - i\mathcal{S}(\xi) \quad (9g)$$

The quantities  $\mathcal{C}(\xi)$  and  $\mathcal{S}(\xi)$  are the Fresnel cosine and sine integrals, and will be evaluated numerically by the formulas derived by Boersma.<sup>12</sup> The final representation for the unsteady surface pressure  $p(x_1, t)$  assumed to be a real quantity, is

$$p(x_1, t) = \Re\{\Delta P(x_1, t)\} \quad (9h)$$

Note that Eqs. 9(a-h) represent the pressure distribution on the upper surface of the airfoil and that this pressure is assumed to be antisymmetric between the upper and lower surfaces. Note, also, some differences between Eqs. 9(e-f) and their counterparts in Refs. 3 and 8. Such differences include the choice of coordinate-axes origin and the spatial normalization employed by the author. Another difference arises from the use of complex conjugates here, which serves to make the present notation more consistent with the eventual broadband representation in Ref. 8, which is also employed in the Section 4. The above surface pressure was originally proposed in order to derive an expression for unsteady lift which was ultimately incorporated into a frequency-domain acoustic formulation.<sup>3,8,13</sup> However, in the present work, the unsteady pressure itself will be used as input to Eq. 6 for a time-domain prediction.

### 3.2 Grid Refinement Study

The surface pressure in Eqs. 9(a-h) is now used to numerically demonstrate the equivalence of Formulation 1B and the loading-noise terms of Formulation 1A<sup>5</sup>. Formulation 1A forms the basis of WOP-WOP, a rotor noise prediction code developed at NASA Langley Research Center.<sup>14</sup> For the prediction of loading noise from an airfoil in uniform rectilinear motion, Formulation 1A simplifies to

$$\begin{aligned} 4\pi p'(\vec{x}, t) = & \int_{\vec{r}_1 > 0} \left[ \frac{\partial p / \partial \tau \cos \theta}{c_0 r (1 - M_r)^2} \right]_{\text{ret}} dS \\ & + \int_{\vec{r}_1 > 0} \left[ \frac{p \cos \theta}{r^2 (1 - M_r)^2} \right]_{\text{ret}} dS \\ & - \int_{\vec{r}_1 > 0} \left[ \frac{p \cos \theta (M_r - M^2)}{r^2 (1 - M_r)^3} \right]_{\text{ret}} dS \end{aligned} \quad (10)$$

Note that the entire formulation here is integrated on the surface interior. At first glance, the form of Eq. 10 appears no more complex than Eq. 6, but only because of the simplicity of uniform, rectilinear motion. Eq. 10, as written above, is not applicable to a rotating surface, but Eq. 6 is. The loading-noise terms of the full Formulation 1A are, indeed, applicable to rotational flow, but the full formulation is more complex than Eq. 10.

The far-field noise radiated from a thin airfoil in a one-dimensional, single-frequency sinusoidal gust is now calculated, using Eq. 6 and Eq. 10. Let  $p'_{1B}$  and  $p'_{1A}$  denote the sound calculated by Eqs. 6 and 10, respectively. If the input surface pressure  $p(\vec{y}, t)$  is known analytically at any point on the airfoil surface, then the only non-machine-zero error made in the numerical solution of Eqs. 6 and 10 is the error associated with the quadrature formula that is chosen to perform the surface and contour integrations. In this case, the mid-point rule is the quadrature of choice. Therefore, the equivalence of Eqs. 6 and 10 is demonstrated if the difference  $|p'_{1B} - p'_{1A}|$  diminishes in mesh refinement like

the cumulative error expected from the mid-point rule, *i.e.* that the error is  $O(\Delta x^2)$ .

The plate's rectangular dimensions are determined by a chord length of  $L_c = 0.5$  meter and a span of  $2b = 2.0$  meters. The plate is moving at a Mach number of 0.2, and the sound speed is taken to be 343 m/sec. The ambient density  $\rho_0 = 1.23$  kg/m<sup>3</sup>, and the upwash amplitude is  $w_0 = 0.05 U$ , *i.e.* five percent of the free stream. The observer position for this test case is  $\vec{x} = [-1, 0, 1]^T$ , in meters. Fig. 3 roughly depicts this relative observer position, although not to scale.

The calculation is performed for one time period of the surface pressure fluctuation at frequencies of  $f = 25$  Hz and  $f = 1$  kHz, with 32 time-steps in each period. These choices of frequency, at the prescribed observer location, will test both the near-field and far-field equivalence of the two formulations. Note that the transfer functions in Eqs. 9(b,f) are singular at  $x_1 = 0$ , and the spatial derivative of Eq. 9(f) is singular at  $x_1 = L_c$ . Although both singularities are integrable, they would cause the quadrature error to deviate from that of the mid-point rule which, by its definition, requires sufficient smoothness throughout the interval of integration. Therefore, the domain of stream-wise integration is restricted to an interval of the form

$$\varepsilon L_c \leq x_1 \leq (1 - \varepsilon) L_c \quad (11)$$

where  $\varepsilon$  is a small, positive parameter.

Each calculation is performed on a sequence of six surface grids:  $\{10 \times 40\}$ ,  $\{20 \times 80\}$ ,  $\{40 \times 160\}$ ,  $\{80 \times 320\}$ ,  $\{160 \times 640\}$ , and  $\{320 \times 1280\}$ . Grid clustering is performed near the leading and trailing edges of the plate in order to accommodate the parameter  $\varepsilon = 0.02$  on the coarser meshes. The maximum values of  $|p'_{1B} - p'_{1A}|$  during each time period, are shown as a function of the number of grid points on a log-log plot in Fig. 4. The abscissa  $N_x$  is the number of surface elements in  $x_1$ . The dashed line represents a fictitious quantity whose values are specifically calculated to be directly proportional to  $N_x^{-2}$ . Clearly, the slopes of both calculations are visibly parallel to a slope of -2, thereby

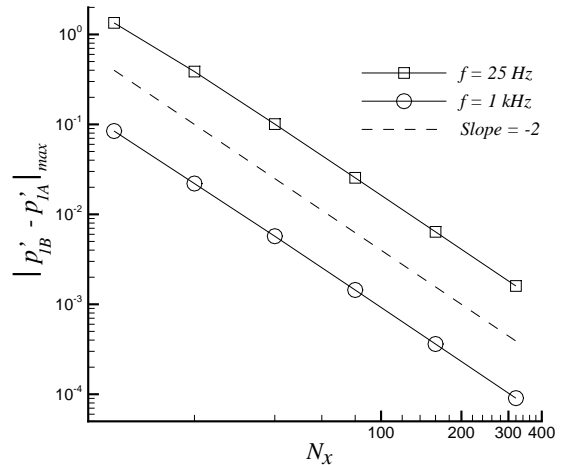


Fig. 4 Grid refinement validation for equivalence of Formulations 1A and 1B.

demonstrating that

$$|p'_{1B} - p'_{1A}| = O(N_x^{-2}) = O(\Delta x_1^2),$$

which is the cumulative error expected from the mid-point rule of integration.

### 3.3 Velocity Scaling Laws

Attention is now turned to the way in which the intensity of the far-field noise, as predicted by Eqn. 6, will scale as a function of velocity, when the surface pressure is described by Eqs. 9(a-h). The physical dimensions of the plate for this exercise are the same as for the test case above. The conditions of a far-field observer in a low-Mach-number flow (Eq. 7) will be assumed. The Mach-number range of interest is  $0.01 \leq M \leq 0.2$ . In addition, the proportionality of the acoustic intensity to velocity will be determined according to two different conditions placed on the frequency  $f$ . These two conditions will delineate between compact and non-compact sources.

First, it will be assumed that the source is compact, *i.e.*  $L_c \ll \lambda$ . This condition will be achieved by requiring the frequency to be proportional to velocity,  $f \sim U/L_c$ , for a sufficiently low range of frequency. For  $0.01 \leq M \leq 0.2$ ,  $f = 80\text{Hz}$  is referenced to  $M = 0.2$ , and  $f$  is then made a function of velocity while requiring a constant Strouhal number  $f L_c/U \approx 0.583$ . The frequency range is, then,  $4\text{Hz} \leq f \leq 80\text{Hz}$ . Note that  $\mu < 0.4$  throughout this range.

The plate's physical dimensions are as in the above mesh refinement problem. The calculation is performed on a  $100 \times 400$  surface grid, with the stream-wise integration interval restricted as in Eq. 11, with sufficient grid clustering near the leading and trailing edges to allow for  $\varepsilon = 0.003$ . The observer is chosen at a distance of 100 meters, directly above the plate's center, *i.e.*  $\vec{x} = [0.25, 0, 100]^T$  in meters. This location places the observer in the acoustic far-field for the entire range of frequency.

A separate calculation is run for each Mach number and its corresponding frequency. The upwash amplitude is  $w_0 = 0.05 U$  for each of 50 equally spaced Mach numbers between 0.01 and 0.2. The surface pressure in Eqs. 9(a-d,h) is used as input to equation to Eq. 6 to predict the far-field sound  $p'(\vec{x}, t)$ . Each calculation is performed for one acoustic period  $T$  of the corresponding frequency, with 64 time-steps. The average intensity  $I(\vec{x})$  of the acoustic signal at the observer  $\vec{x}$ , assuming spherical spreading, is then calculated by

$$I(\vec{x}) = \frac{1}{T} \int_0^T \frac{[p'(\vec{x}, t)]^2 dt}{\rho_0 c_0}$$

The average acoustic intensities for a compact source, as a function of Mach number, are represented as squares in Fig. 5. The slope of these results on a log-log plot can be visually determined by proximity to the dotted line whose slope is precisely six at every point. This  $U^6$  proportionality is consistent with Curle's<sup>4</sup> result, as expected from the conditions placed upon the calculations.

The demonstration of a velocity scaling law is now desired for a non-compact source *i.e.* for  $\mu > 0.4$ . Therefore, the restriction that  $f \sim U/L_c$  must be lifted, so that  $f$  is

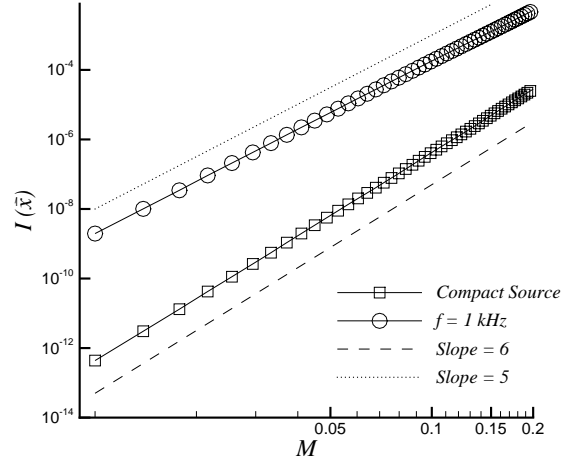


Fig. 5 Velocity scaling properties of Formulation 1B.

independent of  $U$ . The simplest such condition is that  $f$  is constant, in which case the Strouhal number remains a function of  $U$ . A series of calculations is again performed, as above, with the only parameter change being that the frequency is held constant at 1 kHz throughout the range of Mach number. The input surface pressure for this case is given by Eqs. 9(a,e-h). The computed acoustic intensities at 100 meters are represented by circles in Fig. 5. In this case, the acoustic intensity scales approximately as  $U^5$ , a result that is consistent with Ffowcs Williams and Hall<sup>7</sup>.

### 3.4 Directivity

As a final exercise in this section, the directivity of a single-frequency source is examined. The radiated noise  $p'(\vec{x}, t)$  is calculated at many locations on a circular arc in the plane  $x_2 = 0$  that is centered on the geometric center of the plate's upper surface, as shown in Fig. 6. The arc trajectory  $(r, \psi)$  is determined by  $r = 3$  meters and  $0 \leq \psi \leq \pi$ . The directivity is determined by the peak pressure amplitude  $\|p'\|$  that is calculated at each position on the circular arc, during one period in time for a given frequency. The flat plate's dimensions and surface discretization are as in

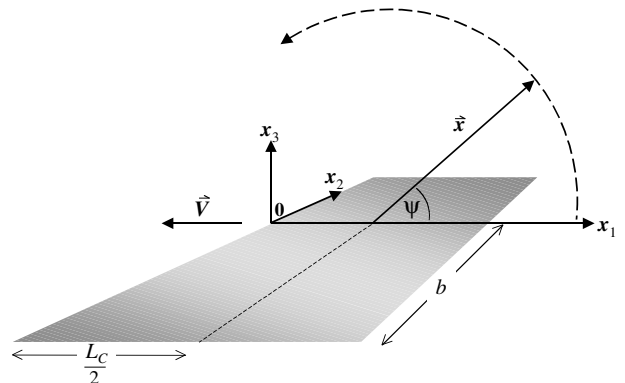
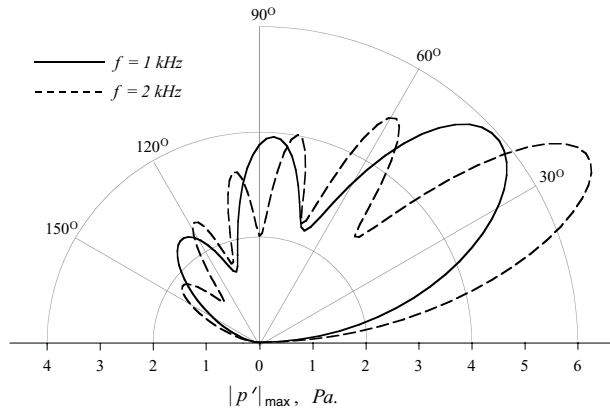


Fig. 6 Schematic for directivity calculation. Observer on circular path in plane  $x_2 = 0$ .



**Fig. 7** Directivity for two sources of constant frequency. 2-kHz results are scaled by a factor of 2.5.

the previous example, and there are 128 time-steps in a period. The observer path,  $0 \leq \psi \leq \pi$ , is discretized into 128 equally spaced locations. The free-stream Mach number is 0.2 and the gust amplitude is  $w_0 = 0.05 U$ . Fig. 7 shows the results, in polar form, for frequencies of 1 kHz and 2 kHz. The higher-frequency results are scaled in order to visualize both loci on the same plot. As expected, there are twice as many lobes in the 2-kHz solution. Also, note the frequency-dependent positions of the lobes with respect to a fixed observer. For example, an observer at  $\psi = \pi/2$  will receive a signal that is near the peak amplitude for the central lobe of the 1-kHz signal, whereas the 2-kHz signal is near a local minimum for the same observer. This frequency-dependent characteristic of directivity is mentioned here for future reference in the following section.

#### 4. Broadband Prediction with Comparison to Experiment

The analytic surface pressure in the previous section is extended to model a broadband source on a slender airfoil at zero angle of attack. This broadband surface pressure is used as input to Formulation 1B to predict far-field radiation, and the results are compared to experimental measurements. Note that Amiet<sup>15</sup> has previously proposed a broadband solution to this problem in the time domain, using the transfer functions in Eqs. 9(e-g). His resulting solution was a Fourier transform of the frequency-domain solution in Refs. 8 and 13. In the current work, the high-frequency formulation in Section 3 is explicitly extended to a broadband source application with user-specified spectral content.

##### 4.1 Experiment - Incident Turbulence Noise

The experiment that is modeled in this section is reported by Paterson and Amiet in Ref. 8. A NACA 0012 airfoil is placed between two vertical plates, at zero angle of attack, in the test section of an open-jet wind tunnel. The airfoil has a chord length of 0.23 m and a span of 0.53 m. Turbulence is generated by a grid upstream of the airfoil. Noise propagates from the test section into an anechoic chamber that is instrumented with six microphones. The microphones are located on the tunnel centerline, on an arc of radius 2.25 m, relative to the airfoil's geometric center. The microphone locations on this arc are at angles of 70, 90, 105, 120, 130, and 140 degrees, relative to the

upstream direction. Far-field noise measurements of the incident turbulence on the airfoil are determined by subtracting microphone measurements, with and without the model, at each of five tunnel speeds: 40, 60, 90, 120, and 165 m/s.

##### 4.2 Broadband Analysis

For prediction purposes, the airfoil is modeled as a flat plate in a periodic gust that gives rise to an unsteady surface pressure that is a broadband extension of the analytic formulation in Section 3. The airfoil geometry is oriented with respect to the coordinate axes as in Fig. 3, with  $\{0 \leq x_1 \leq L_c\} \times \{-b \leq x_2 \leq b\}$ , where  $L_c = 0.23$  m and  $2b = 0.53$  m. As encountered by the airfoil surface in the  $x_1$ - $x_2$  plane, the normal component of the turbulent velocity field can be written

$$w(x_1, x_2, t) = \int_{-\infty}^{\infty} \int_{-\infty}^{\infty} \hat{w}(k_1, k_2) e^{-i[k_1(x_1 - Ut) + k_2 x_2]} dk_1 dk_2$$

where  $\hat{w}(k_1, k_2)$  is the gust amplitude wave-number spectrum, defined by the inverse Fourier transform of  $w(x_1, x_2, t)$ . The complex-valued, unsteady surface pressure arising from the incidence of a turbulent velocity field of this form is given by

$$\Delta P(x_1, x_2, t) = \rho_0 U \int_{-\infty}^{\infty} \int_{-\infty}^{\infty} \hat{w}(k_1, k_2) g(x_1, k_1, k_2) e^{i(k_1 U t - k_2 x_2)} dk_1 dk_2 \quad (12)$$

The expression for surface pressure in Eq. 13 is simplified by the following reasoning. Amiet argues in Ref. 13 that, for an observer in the plane  $x_2 = 0$ , the only spanwise wavenumber that contributes significantly to the far-field sound is  $k_2 = 0$ . His conclusion is derived mathematically, in the frequency domain, for the limiting case of an airfoil of infinite span. From a physical standpoint, this conclusion makes sense for an observer in a location that is symmetric to the airfoil span. The effect on the far-field acoustics of any gust that is skewed to the airfoil leading edge by some angle  $\alpha$  will be canceled by another gust skewed at an angle of  $-\alpha$ . In the case of a finite-span airfoil, Amiet argues that this simplification is still valid as the quantity  $M k_1 b$  becomes large. *i.e.* in the high-frequency limit. Following this line of reasoning, the  $x_2$  dependence in  $\Delta P$  also vanishes, by Eq. 12, and the surface pressure becomes

$$\Delta P(x_1, t) = \rho_0 U \int_{-\infty}^{\infty} \hat{w}(k_1, 0) g(x_1, k_1, 0) e^{i(k_1 U t)} dk_1 \quad (13)$$

The evaluation of the surface pressure in Eq. 13 is accomplished by first recognizing the turbulent fluctuations as a stochastic process. This process can be approximated by a truncated series whose limit exhibits the required relationship between the autocorrelation and the power spectrum of that process. (See, for example, Ref. 16.). This relationship is achieved by evaluating the spectral amplitudes  $\hat{w}(k_1, k_2)$  as a function of the power spectral density (PSD) of  $w(x_1, x_2, t)$ . To this end, the infinite wave-number domain,  $-\infty < k_1 < \infty$ , in Eq. 13 is integrally discretized and truncated such that  $k_{1,-N} < k_{1,n} < k_{1,N}$ . The largest wave number  $k_{1,N}$  represents an “upper-cut-off” wave number, beyond which the spectral density amplitude is considered

negligible or is out of range of experimental measurement. The unsteady surface pressure in Eq. 13 is then approximated by

$$\Delta P(x_1, t) \approx \rho_0 U \sum_{-N}^N A_{n,0} e^{i\Phi_n} g(x_1, k_{1,n}, 0) e^{i(k_{1,n} U t)} \quad (14a)$$

$$k_{1,n} = n \Delta k_1, \quad n = 0, \pm 1, \pm 2, \dots, \pm N$$

$$\Delta k_1 = k_{1,N}/N$$

The phase angles  $\{\Phi_n\}$  are independent random variables uniformly distributed on  $[0, 2\pi]$ . The transfer function  $g(x_1, k_{1,n}, 0)$  is an extension of the high-frequency function in Eqs. 9(e-g), and takes the slightly modified form

$$g(x_1, k_{1,n}, 0) = (g_1 + g_2) e^{-i[2\mu_n(1-M)x_1/L_c + \pi/4 - \bar{k}_{1,n}]}$$

where  $g_1$  and  $g_2$ , now functions of  $k_{1,n}$ , are otherwise identical to Eq. 9(f),

$$g_1(x_1, k_{1,n}) = \frac{1}{[2\pi \bar{k}_{1,n} x_1 (1+M)/L_c]^{\frac{1}{2}}} \quad (14b)$$

$$g_2(x_1, k_{1,n}) = \frac{-1 + (1+i) E^*[4\mu_n(1-x_1/L_c)]}{[2\pi \bar{k}_{1,n} (1+M)]^{\frac{1}{2}}}$$

and  $E^*$  is the same complex combination of Fresnel integrals as in Eq. 9(g). The low-frequency transfer function is not used in these broadband predictions because the experimental facility is anechoic for frequencies above 200 Hz, and the parameter  $\mu$  is greater than 0.4 at this frequency or above, for all five tunnel speeds.

The spectral coefficients  $\{A_{n,0}\}$  are evaluated by

$$A_{n,0} = [S_{ww}(k_{1,n}, 0) \Delta k_1 \Delta k_2]^{\frac{1}{2}} \quad (14c)$$

where  $S_{ww}(k_1, k_2)$  is the two-component power spectral density of  $w$ . As this grid-generated turbulence is assumed to be homogeneous and isotropic, the PSD is evaluated by the von Karman formula.<sup>17</sup> The formula for  $S_{ww}(k_1, k_2)$  that is used in the present calculations is derived from von Karman's energy spectrum in Appendix I of Ref. 13.

$$S_{ww}(k_1, k_2) = \frac{4}{9\pi} \frac{\overline{u^2}}{k_e^2} \frac{\hat{k}_1^2 + \hat{k}_2^2}{[1 + \hat{k}_1^2 + \hat{k}_2^2]^{\frac{4}{3}}} \quad (14d)$$

where  $\overline{u^2}$  is the stream-wise turbulent energy, and

$$\hat{k}_i = \frac{k_i}{k_e}, \quad k_e = \frac{\sqrt{\pi}}{\mathcal{L}_1} \frac{\Gamma(\frac{5}{6})}{\Gamma(\frac{1}{3})}, \quad (14e)$$

and  $\mathcal{L}_1$  is the stream-wise integral length scale

$$\mathcal{L}_1 = \int_0^\infty R_{ww}(x_1) dx_1$$

where  $R_{ww}$  is the upwash correlation function defined by

$$R_{ww}(r) = \frac{w(x_1, t) w(x_1 + r, t)}{w(x_1, t) w(x_1 + r, t)}$$

$$= \lim_{T \rightarrow \infty} \frac{1}{T} \int_0^T w(x_1, t) w(x_1 + r, t) dt$$

Note that the two-component formula in Eq. 14(d) was derived in Ref. 13 by integrating the von Karman energy spectrum over all  $k_3$  components. The  $k_2$  component is

then set to zero for the present calculations. Values for  $\overline{u^2}$  and  $\mathcal{L}_1$  are determined by measurement. In Ref. 18, Fink reports that the turbulence intensity that results from the grid in question can be approximated by the empirical formula

$$\frac{(\overline{u^2})^{\frac{1}{2}}}{U} = 0.04 \left[ \frac{U}{U_{\text{ref}}} \right]^{-0.2} \quad (14f)$$

where the reference speed is  $U_{\text{ref}} = 60$  m/s. Fink<sup>18</sup> also reports a measured value for the integral length scale as  $\mathcal{L}_1 = 3.175$  cm

All of the above expressions and measurements are incorporated into Eq. 14(a). The final representation for the unsteady broadband pressure on the airfoil's upper surface is then given by the real part of Eq. 14(a). This broadband surface pressure is used as input to Formulation 1B to predict the far-field noise  $p'(\vec{x}, t)$ .

Using symmetry arguments and algebraic manipulation, the indicial bounds for the surface pressure's spectral representation are altered so that the domain includes only positive wavenumbers. The resulting real-valued surface pressure on the airfoil's upper surface can be written

$$p(x_1, t) = 2\rho_0 U \sum_{n=1}^N A_{n,0} [B_n \cos(k_{1,n} U t + \Phi_n - \alpha_n) + D_n \sin(k_{1,n} U t + \Phi_n - \alpha_n)] \quad (15a)$$

where the upwash amplitudes  $A_{n,0}$  are evaluated by Eq. 14(c) and  $S_{ww}(k_1, k_2)$  is described in Eqs. 14(d-f). The quantities  $B_n$ ,  $D_n$ , and  $\alpha_n$  are given by

$$B_n = g_1(x_1, k_{1,n}) + \frac{\mathcal{C}(\xi_n) + \mathcal{S}(\xi_n) - 1}{[2\pi \bar{k}_{1,n} (1+M)]^{\frac{1}{2}}}$$

$$D_n = \frac{\mathcal{S}(\xi_n) - \mathcal{C}(\xi_n)}{[2\pi \bar{k}_{1,n} (1+M)]^{\frac{1}{2}}} \quad (15b)$$

$$\alpha_n = 2\mu_n(1+M) \frac{x_1}{L_c} - \bar{k}_{1,n} + \frac{\pi}{4}$$

where  $g_1(x_1, k_{1,n})$  is evaluated in Eq. 14(b), and  $\mathcal{C}(\xi_n)$  and  $\mathcal{S}(\xi_n)$  are the Fresnel cosine and sine integrals in Eq. 9(g) with  $\xi_n = 4\mu_n(1-x_1/L_c)$ . The summation in Eq. 15(a) begins at  $n = 1$  because  $S_{ww}(0, 0) = 0$ , by Eq. 14(d).

At this point, the value of  $\Delta k_2$  in Eq. 14(c) is unknown because there is no explicit span-wise integration, thereby giving rise to an adjustable constant. This constant is one of scale only, and found to have no effect the shape of the far-field spectrum. Furthermore, this scale factor is found to be constant for all data points, *i.e.* is independent of all parameters considered (tunnel speed, frequency range, band-width, airfoil span, etc.).

### 4.3 Time-Domain Predictions

The lower frequency bound, and therefore the fundamental frequency, for all five calculations is chosen at 10 Hz. The upper frequency for the predictions is chosen according to the upper frequency for which measurements are available for each tunnel speed. For  $U = 40, 60$ , and  $90$  m/s, the upper bound is  $f_N = 2.5$  kHz. The upper bounds for  $U = 120$  and  $165$  m/s are  $f_N = 3.5$  kHz and  $4.5$  kHz, respectively. For all five calculations, the numerical band-width is  $\Delta f = 10$  Hz. Each calculation is performed for one

period of the lowest frequency, *i.e.*  $T = 0.1$  second. The numerical solution is sampled at the Nyquist frequency, *i.e.*  $\Delta t = T/2N$ . The calculation is performed on a  $100 \times 230$  surface grid, with the stream-wise integration interval restricted as in Eq. 11, with sufficient grid clustering near the leading and trailing edges to allow for  $\varepsilon = 0.003$ .

The experimental microphone position for which comparisons are made is at a distance of 2.25 m from the model, and at an angle of 90 degrees relative to the model's geometric center. The coordinate system for the calculation is such that the  $x_2$ -axis is coincident with the center-span line, so that the microphone position is in the plane  $x_2 = 0$ , as in Fig. 6. The measured observer position for the prediction is, then,  $\vec{x} = [0.115, 0, 2.25]^T$  in meters.

The position of the microphone relative to the airfoil is corrected for refraction due to the presence of a shear layer that forms downstream of the upper lip of the square nozzle exit and is positioned between the model and the microphone. This correction is based on geometrical acoustics with an assumption of a zero-thickness shear layer, and is reported in Ref. 19. Shear-layer corrections that are based on such formulations<sup>19</sup> are reasonable for the present case with the microphone directly above the source. The required correction in the microphone position is significant. At a measured angle of 90 degrees, the corrected angles ranged from approximately 84.5 degrees for  $U = 40$  m/s to 68.2 degrees for  $U = 165$  m/s.

In addition, the amplitude of the radiated noise is also corrected for the presence of the shear layer, although at a measured angle of 90 degrees, the amplitude correction is not significant, especially for the lower tunnel speeds. The computed sound pressures  $p'(\vec{x}, t)$  were corrected by factors ranging from approximately 0.997 for  $U = 40$  m/s to 0.942 for  $U = 165$  m/s. The microphone position is corrected for the shear-layer in a pre-processing step. After the far-field noise is calculated at the corrected position, the results are then post-processed for amplitude correction. In this way, the corrected predictions can be compared to the experi-

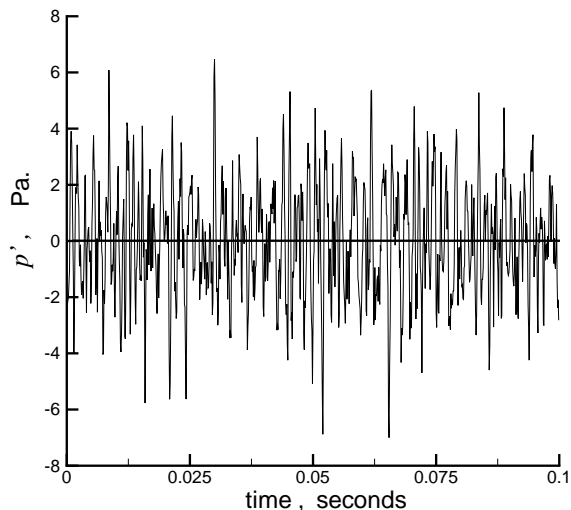


**Fig. 8** Predicted far-field signal,  $U = 165$  m/s. Microphone at  $90^\circ$ , 2.25 m above airfoil center.

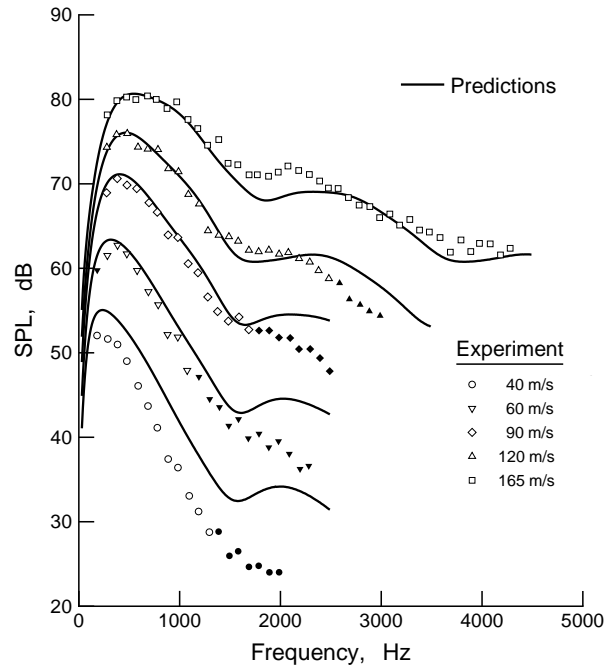
mental results “as measured.”

Fig. 8 shows the far-field signal  $p'(\vec{x}, t)$  that is predicted by Formulation 1B, for one fundamental period in time, at the experimental microphone location, for a tunnel speed of 165 m/s. Shear-layer corrections for amplitude and directivity are included in this plot. In order to compare with experimental measurements in Ref. 8, the time-domain results from the numerical predictions, for all five tunnel speeds, are Fourier analyzed and converted to the frequency domain. The resulting frequency-domain solution,  $p'(f_n)$ , is used to compute the sound pressure level (SPL) spectrum of the far-field radiation. These sound pressure levels are determined by

$$SPL(f_n) = 10 \log \left\{ \frac{p'^2(f_n)}{p_{ref}^2} \right\} \quad (16)$$

where the reference pressure is  $p_{ref} = 2 \times 10^{-5}$  Pa. The SPL's are converted to a 1 Hz band-width by reducing the values in Eq. 16 by  $10 \log(\Delta f)$ . This narrow-band conversion is consistent with the experimental SPL's which were measured at a band-width of 55.7 Hz and reduced by 17.5 dB.<sup>8</sup>

The predicted far-field spectral density for the five tunnel speeds is shown Fig. 9 along with experimental measurements from Ref. 8. The solid symbols represent those measurements for which the difference between the noise with and without the airfoil model was considered too small, and are therefore subject to greater uncertainty. The agreement with the measured data is very good. The noticeable “humps” in the predicted spectra are, most likely, the result of the changing placement of lobes, as a function



**Fig. 9** Predicted and measured far-field noise spectra. Microphone at  $90^\circ$ , 2.25 m above airfoil center. Experimental data reproduced from Ref. 8. Solid symbols denote low signal-to-noise ratio.

of frequency, relative to the observer. This phenomenon was described in Section 3 (Fig. 7). That the current predictions are nearly identical to the predictions in Ref. 8 is not surprising, because the current predictions rely upon the same unsteady surface pressure formulation as those in Ref. 8.

### 5. Statistical Formulation

Often, when aeroacoustic experiments are performed, surface-pressure correlations are extremely useful in characterizing noise due to an airflow over a model. Under certain conditions, Formulation 1B is readily transformed into an expression that aids in statistical analysis of broadband noise. Recall that, in the case of low Mach number and with an observer in the acoustic far field (Eq. 7), the signal is dominated by the first integral in Eq. 6. Also, recall that the spatial and temporal derivatives of pressure in this integral can be written as a single time derivative of pressure when evaluated in a reference frame that is fixed relative to the medium at rest, as in Eq. 5(b). In this fixed reference frame, the far-field sound at low Mach number is approximated by

$$4\pi p'(\vec{x}, t) \approx \int_{\vec{r} > 0} \left[ \frac{\dot{p} \cos \theta}{c_0 r (1 - M_r)} \right]_{\text{ret}} dS \quad (17)$$

In addition, assume that the observer is many correlation lengths into the far field, *i.e.*  $r \gg \ell_i$ , where

$$\ell_i = \frac{1}{R_{ww}(0)} \int_0^\infty R_{ww}(x_i) dx_i, \quad i = 1, 2$$

In this case, the values of  $r$ ,  $M_r$ , and  $\theta$  are nearly invariant within a correlation area  $A_\ell$  of size  $\ell_1$  by  $\ell_2$ , and Eq. 17 can be re-written as

$$4\pi p'(\vec{x}, t) \approx \sum_1^K \frac{\cos \theta_k}{c_0 r_k (1 - M_{r_k})} \int_{A_{\ell_k}} \dot{p}(\vec{y}, \tau) dS \quad (18)$$

where  $r_k$ ,  $\theta_k$ , and  $M_{r_k}$  are constant values chosen to replace their nearly invariant counterparts in retarded time, within each correlation area.

If the autocorrelation operator is applied to Eq. 17, the result is

$$16\pi^2 R_{p'p'}(\bar{\tau}) = 16\pi^2 \overline{p'(\vec{x}, t) p'(\vec{x}, t + \bar{\tau})} \quad (18a)$$

$$\approx \sum_1^K \left[ \frac{\cos \theta_k}{c_0 r_k (1 - M_{r_k})} \right]^2 \int_{A_{\ell_k}} R_{pp}(\vec{y}; \vec{\eta}, \bar{\tau}) d\vec{\eta} d\vec{y}$$

where

$$R_{pp}(\vec{y}; \vec{\eta}, \bar{\tau}) = \overline{\dot{p}(\vec{y}, \tau) \dot{p}(\vec{y} + \vec{\eta}, \tau + \bar{\tau})} \quad (18b)$$

The ability to measure such time-derivative correlations, relative to the medium at rest, is already in hand.<sup>20</sup> The potential usefulness of this alternate formulation is clear. After the autocorrelations in Eq. 18(b) are determined experimentally, and used as input to Eq. 18(a), then the Fourier transform of Eq. 18(a) produces the far-field noise spectrum. The further development and testing of this statistical formulation is a topic of ongoing research for its potential application to trailing edge noise prediction.

### Concluding Remarks

A new formulation for the solution of the loading term of the Ffowcs Williams-Hawkings equation has been derived. The potential usefulness of time-domain solutions for acoustic predictions with Formulation 1B has been demonstrated. This new far-field formulation has some advantages over previous formulations. The formulation is both simple and has broad application, including the case of non-uniform flow. In addition, the dominance of only one term in this formulation makes this solution much easier to pose in correlation-function form for statistical analysis of broadband noise. Such an alternative formulation can be used to aid acoustic experiments where surface pressure correlations are measured.

### Acknowledgements

The authors would like to express their gratitude to Dr. Roy K. Amiet, whose input from his past experience was invaluable to this research. In addition, the authors are grateful to Dr. Meelan Choudhari, of NASA Langley Research Center, for several enlightening discussions.

### References

1. Lighthill, M. J., "On Sound Generated Aerodynamically. I. General Theory," *Proceedings of the Royal Society of London*, A 211, 1952, pp. 564-587.
2. Ffowcs Williams, J. E. and Hawkings, D. L., "Sound Generation by Turbulence and Surfaces in Arbitrary Motion," *Philosophical Transactions of the Royal Society*, A 264, 1969, pp. 321-342.
3. Amiet, R. K., "High Frequency Thin-Airfoil Theory for Subsonic Flow," *AIAA Journal*, Vol. 14, No. 8, 1976, pp. 1076-1082.
4. Amiet, R. K., "Compressibility Effects in Unsteady Thin-airfoil Theory," *AIAA Journal*, Vol. 12, No. 2, 1974, pp. 252-255.
5. Farassat, F. and Succi, G. P., "The Prediction of Helicopter Rotor Discrete Frequency Noise," *Vertica*, Vol. 7, No. 4, 1983, pp. 309-320.
6. Curle, N., "The Influence of Solid Boundaries on Aerodynamic Sound," *Proceedings of the Royal Society of London*, A 231, 1954, pp. 505-514.
7. Ffowcs Williams, J. E. and Hall, L. H., "Aerodynamic Sound Generation by Turbulent Flow in the Vicinity of a Scattering Half-Plane," *Journal of Fluid Mechanics*, Vol. 40, 1970, pp. 657-670.
8. Paterson, R. W., and Amiet, R. K., "Noise and Surface Pressure Response of an Airfoil to Incident Turbulence," *AIAA Journal of Aircraft*, Vol. 14, No. 8, 1977, pp. 729-736.
9. Farassat, F., "Introduction to Generalized Functions with Applications to Aerodynamics and Aeroacoustics," NASA Technical Paper No. 3428, 1994, (Corrected 1996), <http://techreports.larc.nasa.gov/ltrs/PDF/tp3428.pdf>.
10. Farassat, F., "Theory of Noise Generation From Moving Bodies with an Application to Helicopter Rotors," NASA Technical Report R-451, 1975, <http://techreports.larc.nasa.gov/ltrs/PDF/NASA-75-trr451.pdf>.

11. Von Karman, T., and Sears, W. R., "Airfoil Theory for Non-Uniform Motion," *Journal of the Aeronautical Sciences*, Vol. 5, No. 10, 1938, pp. 379-390.
12. Boersma, J., "Computation of Fresnel Integrals," *Math. Comp.*, Vol. 14, 1960, p. 380.
13. Amiet, R. K., "Acoustic Radiation from an Airfoil in a Turbulent Stream," *Journal of Sound and Vibration*, Vol. 41, 1975, pp. 407-420.
14. Brentner, K. S., "Prediction of Helicopter Rotor Discrete Frequency Noise – A Computer Program Incorporating Realistic Blade Motions and Advanced Acoustic Formulation," NASA Technical Memorandum, No. 87721, October 1986.
15. Amiet, R., "Gust Response of a Flat-Plate Airfoil in the Time Domain," *Quarterly Journal of Mechanics and Applied Math*, Oxford University Press, Vol. 39, Part 4, 1986, pp. 485-505.
16. Shinozuka, M., and Deodatis, G., "Simulation of Stochastic Processes by Spectral Representation," *Applied Mechanics Review*, Vol. 44, No. 4, 1991, pp. 191-204.
17. Von Karman, T., "Progress in the Statistical Theory of Turbulence," *Journal of Marine Research*, Vol. 7, No. 3, 1948, pp. 252-264.
18. Fink, M. R., "Experimental Evaluation of Theories for Trailing Edge and Incidence Fluctuation Noise," *AIAA Journal*, Vol. 13, No. 11, 1975, pp. 1472-1477.
19. Amiet, R., "Correction of Open Jet Wind Tunnel Measurements for Shear Layer Refraction," AIAA Paper No. 75-532, 1975.
20. Devenport, W., Virginia Polytechnic Institute and State University, private communication, November 7, 2001.